

# Starbursts in barred spiral galaxies

## IV. On young bars and the formation of abundance gradients \*

S. Considère<sup>1</sup>, R. Coziol<sup>1</sup>, T. Contini<sup>2</sup>, and E. Davoust<sup>3</sup>

<sup>1</sup> Observatoire de Besançon, UPRES-A 6091, B.P. 1615, F-25010 Besançon Cedex, France

<sup>2</sup> European Southern Observatory, Karl-Schwarzschild-Strasse 2, D-85748 Garching bei München, Germany

<sup>3</sup> Observatoire Midi-Pyrénées, UMR 5572, 14 Avenue E. Belin, F-31400 Toulouse, France

Received 20/09/1999; accepted 14/01/2000

**Abstract.** The oxygen (O/H) and N/O abundance ratios along the bar of 16 barred spiral starburst galaxies are determined using long-slit spectroscopy. The abundance gradients and the spatial distribution of the ionized gas along the bar are used to understand the role of bars in starburst galaxies.

The oxygen abundance gradients are steeper than in normal barred galaxies, with a mean of  $-0.15$  dex/kpc, while the intersects are low. This excludes the possibility that starburst galaxies in this sample are chemically evolved galaxies rejuvenated by the effect of a bar. The nitrogen-to-oxygen abundance gradients are flatter than the oxygen ones with a mean of  $-0.05$  dex/kpc. But N/O intersects are high, which rules out the possibility that a large quantity of gas was recently funneled by a bar toward the center of a young galaxy. There is no correlation between the abundance gradients and the bar properties, which suggests that bars did not influence the chemical evolution of these galaxies. Therefore, bars cannot be at the origin of the bursts in the nuclei of our sample galaxies.

The oxygen and N/O abundance gradients are generally stronger in the bar than in the disk and are linked together by a linear relation consistent with a *primary* + *secondary* origin for the production of nitrogen. This can be fully explained in terms of star formation history in these galaxies. The gradients build up from the inside out, becoming stronger as the oxygen and N/O abundances increase in the bulge while staying low in the disk. This behavior is consistent with a simple Schmidt law relating the density of star formation to that of gas.

In many of the sample galaxies, star formation occurs at one or both ends of the bar. The low level of chemical enrichment in these regions suggests that they recently experienced bar-triggered star formation: this is the only visible effect of bars. Our analysis shows that bars probably appeared very recently (a few  $10^7$  years) in the starburst galaxies, which are relatively “young” galaxies still in the process of formation.

**Key words:** Galaxies: abundances – Galaxies: spiral – Galaxies: starburst

### 1. Introduction

Massive galaxies play a fundamental role in the chemical evolution of the Universe, because they are the only systems which meet the physical conditions necessary for the build-up of heavy elements. Today, by using simple techniques and modest-size telescopes, it is possible to understand how the production of metals occurs in nearby massive galaxies and to relate this production to their formation and evolution processes.

While still in its early stages, the study of chemical abundances in external galaxies has already produced important results. One of the most interesting is the discovery that galaxies in the Universe seem to follow a mass-metallicity relation (Zaritsky et al., 1994). Although we still have to understand the physical causes behind this behavior, there is no doubt that this phenomenon is a key parameter for understanding galaxy evolution. With this prospect in mind, we recently verified that the massive starburst nucleus galaxies (SBNGs) follow the same mass-metallicity relation as normal ones (Coziol et al., 1997a). Our observations not only confirm the universality of the mass-metallicity relation for a wide range of galaxies, but also suggest that its origin may be linked to the different paths followed by early and late-type spiral galaxies to form their bulge and disk (Coziol et al., 1998).

Another important phenomenon, unveiled by chemical abundance studies, is that the metallicity in the ionized interstellar medium of spiral galaxies decreases outward (e.g. Vila-Costas & Edmunds, 1992, and references therein). Various hypotheses have been proposed to explain this gradient (Pagel, 1989; Götz & Köppen, 1992), but their verification is difficult. The reason is that many parameters and processes involved in the formation of an abundance gradient are still not well understood, such as the initial mass function, the yield, the mechanisms and time scales for the formation of halos, bulges and disks, as well as the possible infall or outfall of matter. Different numerical simulations have shown, however, that one

Send offprint requests to: considere@obs-besancon.fr

\* Based on observations obtained at the 193cm telescope of Observatoire de Haute-Provence, operated by INSU (CNRS)

important ingredient for producing abundance gradients is a non linear dependence of the star formation rate on gas density (Wise & Silk, 1989; Götz & Köppen, 1992; Mollá et al., 1996). It has also been suggested that once an abundance gradient is established, the presence of gas flows can either amplify or reduce it (Edmunds, 1990; Götz & Köppen, 1992).

Attempts to relate abundance gradients to other characteristics of galaxies, such as morphological type, luminosity or circular velocity, have also been performed (Vila-Costas & Edmunds, 1992; Oye & Kennicutt, 1993; Zaritsky et al., 1994), but no clear correlation has emerged. One interesting trend is however observed: barred spiral galaxies seem to have shallower abundance gradients than non-barred ones (Vila-Costas & Edmunds, 1992; Edmunds & Roy, 1993; Zaritsky et al., 1994; Martin & Roy, 1994). From a theoretical point of view, bars are expected to funnel gas from the outer parts to the nuclei of galaxies (Noguchi, 1988). The flow along the bar can induce strong mixing (Friedli et al., 1994) and reduce metallicity gradients. But star formation induced by the bar can also be strong enough to counteract dilution effects and increase the gradient in the inner parts of galaxies. Steep abundance gradients have indeed been reported in the inner parts of some barred galaxies, such as NGC 3359 (Martin & Roy, 1995) and NGC 1365 (Roy & Walsh, 1998).

In the present paper, we analyse the abundance gradients of oxygen (O/H) and nitrogen to oxygen ratio (N/O) in 16 barred starburst galaxies. Our goal is to establish if starburst galaxies follow the trends observed in normal galaxies. We also want to determine if there is a relation between the bar and the burst of star formation. We have recently proposed that SBNGs may be “young” galaxies still in their formation process (Coziol et al. 1997a, 1998). This possibility raises several new questions. Is the initial distribution of abundances in starburst galaxies flat, or have they already had enough time to establish steep gradients? Is it possible to determine how the gradient builds up in a young galaxy and establish whether the presence of the bar is important? Could bars be younger in starburst than in normal galaxies?

Our analysis innovates by studying the abundance gradients of two key elements, oxygen and nitrogen, which are assumed (Coziol et al., 1999a) to be produced by different types of stars and, thus, to be released into the interstellar medium on different time scales. This gives us a deeper insight into the processes of chemical evolution, because we can test the influence of star formation and of structures, like a bar, over a relatively long period of time (a few Gyrs). This advantage should in particular enable us to determine whether bars are young and if they play a major role in triggering or feeding the nuclear starbursts.

## 2. The sample of barred starburst galaxies

The 16 galaxies studied in this paper are a sub-sample of 144 Markarian barred spiral galaxies studied spectroscopically by Contini (1996) and Contini et al. (1998) (Paper III). This sub-sample is a selection of galaxies which are experiencing very intense bursts of star formation, as estimated by their high

**Table 1.** Catalogue elements of the sample galaxies and excerpts from our observing logbook

Galaxy	Type	$D$ [Mpc]	$r_{25}$ [ $''$ ]	Exp. [min]	P.A. [deg]
Mrk 2	SB0/a	76	23.3	45	66
Mrk 12	SABc	56	36.1	40	32
Mrk 13	SBb	22	34.4	40	128
Mrk 306	SBbc	77	36.1	90	7
Mrk 307	SBc	76	34.4	90	22
Mrk 326	SABbc	49	52.1	45	111
Mrk 332	SBc	34	44.3	90	100
Mrk 373	SBc	81	21.7	90	20
Mrk 545	SBA	63	64.1	90	159
Mrk 602	SBbc	38	40.5	90	33
Mrk 710	SBab	20	67.1	30	33
Mrk 712	SBbc	62	33.7	45	8
Mrk 799	SBb	43	68.7	3×25	144
Mrk 898	SBbc	70	32.9	45	147
Mrk 1076	SBbc	96	24.4	90	148
Mrk 1088	SB0/a	61	55.9	90	25
NGC 6764	SBbc	36	73.6	16,25	62,74

$H\alpha$  luminosity ( $L(H\alpha) > 10^{40}$  erg s $^{-1}$ ) or large  $H\beta$  equivalent width ( $EW(H\beta) > 30$  Å). Three Wolf–Rayet galaxies are included in our sample: Mrk 710, 712 and 799. Another Wolf–Rayet galaxy satisfying our selection criteria, NGC 6764, (Contini et al., 1997), was later added to the list; but, as we will show later, it turns out to be a LINER and cannot be included in our analysis.

Some catalog elements for the sample galaxies and excerpts from our observing logbook are presented in Table 1. The morphologies were taken in NED (<http://nedwww.ipac.caltech.edu>), or in LEDA (<http://www-obs.univ-lyon1.fr>) for Mrk 13 and 306. Table 1 also lists the distance  $D$ , estimated from the recession velocity (assuming  $H_0 = 75$  km s $^{-1}$  Mpc $^{-1}$ ), and the radius  $r_{25}$  at 25 mag arcsec $^{-2}$ . Both values were found in LEDA. The last two columns indicate the exposure times and position angles of the slit which were used during our spectroscopic observations.

## 3. Spectroscopic observations and reductions

Most of the spectroscopic observations were obtained in October 1995 and June 1996 at the 1.93 meter telescope of Observatoire de Haute-Provence. The CCD was a thinned 512×512 Tektronix (pixel size 27 $\mu$ m). We used the Carelec spectrograph (Lemaître et al., 1990) with a spectral dispersion of 260 Å/mm, which covers the spectral range 3600 to 7200 Å, at a resolution of  $\sim 7$  Å. The slit was aligned along the bar. During the first run, we took 90-minute spectra of most galaxies, with a slit width of 3.0 $''$ . For flux calibration, we observed the standard stars G191B2B, Hilt 600, HD 217086 and BD +28° 4211 (Massey et al., 1988). In the second run, we took three 25-minute spectra of Mrk 799 and two of NGC 6764, with a slit width of 2.8 $''$ .

One standard star, HD 192281, was used for flux calibration (Massey et al., 1988). The galaxies Mrk 710 and 712 were observed during previous runs at the same telescope, using similar instrumental settings (Contini et al., 1998). The average seeing during the nights was of the order of  $1.2''$ .

All spectra were reduced with MIDAS, applying standard procedures: offset and flatfield corrections, sky subtraction, wavelength and flux calibration, airmass and galactic extinction corrections and elimination of cosmic impacts. In order to study abundance variations along the bar, series of one-dimensional spectra were extracted from the two-dimensional spectra of each galaxy by averaging three contiguous rows along the slit. Observed emission-line fluxes and equivalent widths were then measured in each elementary spectrum. For the rest of the reduction we followed the procedure outlined in Contini et al. (1995) (Paper I): the Balmer ( $H\alpha$  and  $H\beta$ ) absorption contamination due to underlying stellar populations was corrected by adding  $2\text{\AA}$  to the equivalent width of the Balmer emission lines; the principal Balmer decrement ( $H\alpha/H\beta$ ) was used to estimate the reddening coefficient  $c_{H\beta}$  and to calculate absolute dereddened fluxes.

Our analysis may differ from other studies found in the literature, because we measured the spatial variations of physical parameters only along one direction (along the bar), and not across the whole two-dimensional disk. This difference should be kept in mind when comparing our results with those of other studies.

#### 4. Properties of emission-line regions

A standard diagnostic diagram (Baldwin et al., 1981; Veilleux & Osterbrock, 1987) was used to determine the dominant source of excitation of the emission-line regions in our sample. Most of these regions fall in the domain of HII region-like spectra (Fig. 1), referred to hereafter as HII regions. The only exceptions are two regions in Mrk 545, which have weak signal-to-noise ratios, and the inner region of NGC 6764. There has been some confusion in the literature about the nature of the activity in this last galaxy (see Contini et al. 1996 for the various classifications). Our new spectra clearly show that the center of NGC 6764, as well as the circum-nuclear regions, are the seat of LINER activity. Because LINER is a non-thermal phenomenon (implying either an AGN or shocks), the metallicity in these regions cannot be determined by the methods used in this paper. Consequently, NGC 6764 (and the two regions in Mrk 545) have been excluded from our abundance gradient analysis.

Our sample of HII regions spans a large range of excitation levels, from high-excitation spectra ( $\log ([\text{O III}]/H\beta) \geq 0.4$ ), characteristic of HII galaxies, to low-excitation spectra ( $\log ([\text{O III}]/H\beta) < 0.4$ ) typical of SBNGs (Coziol, 1996). The low-excitation HII regions have  $[\text{N II}]\lambda 6584/H\alpha$  ratios which are relatively high. This is a common property of SBNGs (Coziol et al., 1997b; Contini et al., 1998), which possess a slight overabundance of nitrogen as compared to HII regions with comparable metallicity (Coziol et al., 1999a).

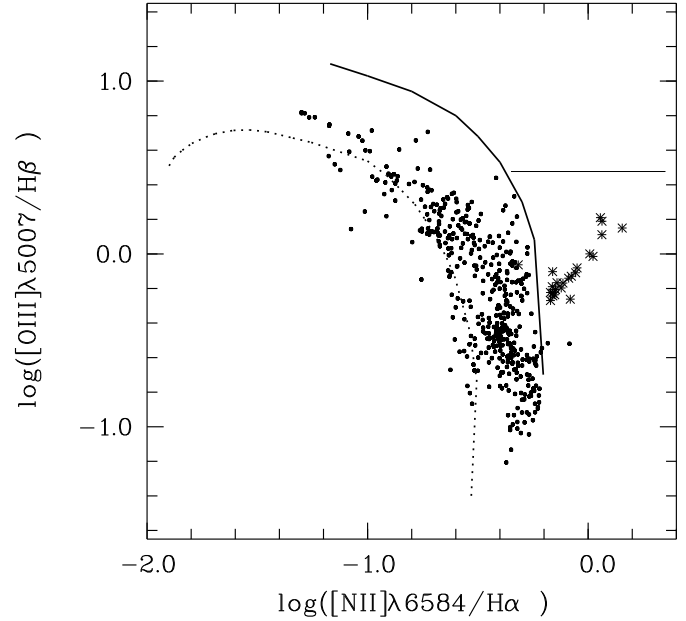


**Fig. 1.** Diagnostic diagram for the emission-line regions of the 17 sample galaxies. The curved solid line separates HII region-like objects (*left*) from active galaxies (*right*). The horizontal solid line separates Seyfert 2 nuclei (*top*) and LINERs (*bottom*). The dotted curve denotes the theoretical model of disk HII region of McCall et al. (1985). Most of the emission-line regions are of HII type, except those located in the central part of NGC 6764 which are of LINER type (*asterisks*)

#### 5. Determination of oxygen and nitrogen abundances

##### 5.1. Determination of oxygen abundances: general method

The oxygen abundances are determined using empirical relations between  $\log(\text{O}/\text{H})$  and the emission-line ratios  $R_3$  and  $R_{23}$ , which are defined as:

$$R_3 = ([\text{O III}]\lambda 4959 + [\text{O III}]\lambda 5007)/H\beta \quad (1)$$

$$R_{23} = ([\text{O II}]\lambda 3727 + [\text{O III}]\lambda 4959 + [\text{O III}]\lambda 5007)/H\beta \quad (2)$$

For our analysis we use the empirical relations first established by Edmunds & Pagel (1984) and quantified by Vacca & Conti (1992). In general, the above two relations yield similar results. In some cases, however, the relation based on  $R_3$  gives higher oxygen abundances than the one based on  $R_{23}$ , because the extinction correction affects differently the two relations; a high extinction correction tends to decrease the ratio  $R_3$ , while increasing the ratio  $R_{23}$ . The consequence of this effect is that when dust extinction is high, one overestimates the oxygen abundance using  $R_3$  and underestimates it using  $R_{23}$ . For this reason, we will use both relations and adopt the mean value. Exceptions are Mrk 710 and 712, where  $[\text{O II}]\lambda 3727$  was not observed and only  $R_3$  was used.

### 5.2. Determination of extinction in the center of galaxies

In the center of half of the sample galaxies (Mrk 12, 307, 326, 332, 545, 799, 898 and 1088), Balmer absorption features due to an underlying intermediate-age stellar population severely affect the measurement of the Balmer emission lines. This prevents us from determining the extinction coefficient  $c_{H\beta}$  which is needed for calculating the abundances. The standard correction of  $2\text{\AA}$  on the equivalent width is not adequate for these cases (because we still cannot measure  $H\beta$  correctly) and it is thus necessary to find a more suitable method to solve this problem.

It has been known for some time that there is an empirical relation between  $\log(R_3)$  and  $\log([N II]/[O III])$  (Alloin et al., 1979; Edmunds & Pagel, 1984). The advantage of using the  $[N II]$  and  $[O III]$  emission lines for determining the oxygen abundance is that they are not affected by underlying stellar populations. Such a method is ideal for analyzing the central regions of galaxies. However, we still have to correct these lines for dust extinction. As we will now show, this can be done empirically.

According to the definition of the extinction coefficient, the observed and dereddened fluxes of the  $[N II]\lambda 6584$  and  $[O III]\lambda 5007$  lines (hereafter  $[N II]$  and  $[O III]$ ) are linked by the relation:

$$\log [N II]/[O III]_{dred} = \log [N II]/[O III]_{obs} - 0.3 \times c_{H\beta} \quad (3)$$

If one plots  $\log([N II]/[O III])_{dred}$  versus  $\log([N II]/[O III])_{obs}$  for a sample of spectra, statistically large enough to include evenly distributed values of  $c_{H\beta}$  between 0.0 and  $\sim 1.5$ , one expects the data to cover uniformly the region between the line of zero extinction and that of  $c_{H\beta} \sim 1.5$ . We notice instead that the data gather along an oblique line of slope smaller than unity, which intersects the lines of constant  $c_{H\beta}$  (see Fig. 2). This is observed in two samples of HII regions in normal galaxies (McCall et al., 1985; Vila-Costas & Edmunds, 1993), as well as in our own sample of starburst galaxies (excluding the spectra affected by Balmer absorption). This correlation translates the fact that, on average, the larger the value of  $\log([N II]/[O III])$  the larger that of  $c_{H\beta}$ . The reason behind this behavior is that  $\log([N II]/[O III])$  is correlated with oxygen abundance (see Sect. 5.3 and Fig. 3), which in turn is correlated with the amount of dust and consequently with internal extinction (Heckman et al., 1998).

This observed correlation provides us with an empirical way of estimating  $c_{H\beta}$  from the observed fluxes of  $[N II]$  and  $[O III]$ . Using the sample of galaxies of McCall et al. (1985) and our own sample (excluding the spectra with Balmer absorption), we find the following relation between the observed and dereddened line ratios:

$$\log([N II]/[O III])_{dred} = 0.93 \log([N II]/[O III])_{obs} - 0.16 \quad (4)$$

The correlation coefficient of this relation is 0.99 and the uncertainty on  $\log([N II]/[O III])_{dred}$  is less than 0.1 dex. This re-

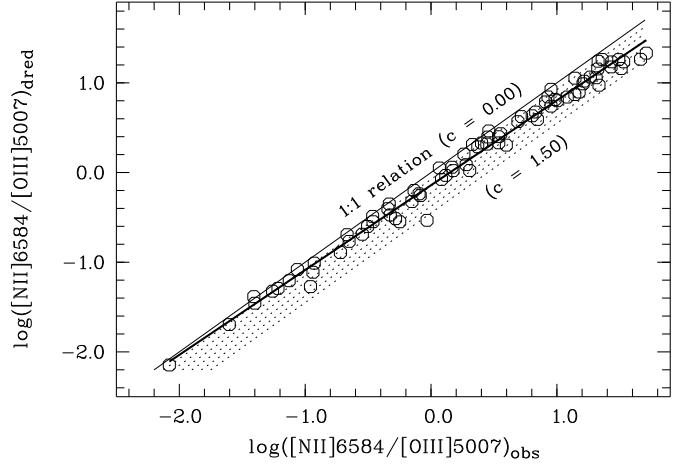


**Fig. 2.** Dereddened versus observed flux ratios of  $[N II]\lambda 6584$  and  $[O III]\lambda 5007$ . The thin line is a 1 to 1 relation. A set of dotted parallel lines represents 6 ranges of  $c_{H\beta}$  varying from 0.25 to 1.50 (see text). The sample of normal galaxies of McCall et al. (1985) is used as an example (open circles). The thick line is the regression on the data

lation will be used in Sect. 5.3 to calculate  $([N II]/[O III])_{dred}$ , and thus  $R_3$ , in the center of galaxies affected by Balmer absorption.

Using the same samples, we find the following relation between  $c_{H\beta}$  and  $([N II]/[O III])_{obs}$ :

$$c_{H\beta} = 0.45 \log([N II]/[O III])_{obs} + 0.51 \quad (5)$$

The correlation coefficient is about 0.95 and the uncertainty is about 0.1 in  $c_{H\beta}$ . This relation will be used in Sect. 5.4 to deredden the  $[O III]\lambda 5007$ ,  $[O II]\lambda 3727$  and  $H\alpha$  lines in the center of galaxies with strong Balmer absorption, and hence to calculate  $R_{23}$ .

### 5.3. Calculating $R_3$ in the center of galaxies

Following an idea developed by various authors (Alloin et al., 1979; Edmunds & Pagel, 1984), we now search for an empirical relation between  $R_3$  and  $[N II]/[O III]$  in our sample of 16 barred starburst galaxies. For this analysis we use only the dereddened fluxes of HII regions, about 300 of them, which are not affected by Balmer absorption. The two quantities appear to be strongly correlated, as shown on Fig. 3a, and we fit a two-degree polynomial to the data, which yields the following relation:

$$\log(R_3) = -0.123 (\log([N II]/[O III]))^2 - 0.661 \log([N II]/[O III]) + 0.086 \quad (6)$$

with a dispersion in  $\log(R_3)$  equal to 0.07 dex.

To check the validity and the possible “universality” of the above relation, we now apply the same procedure to two samples of HII regions in normal galaxies: those of McCall et al.

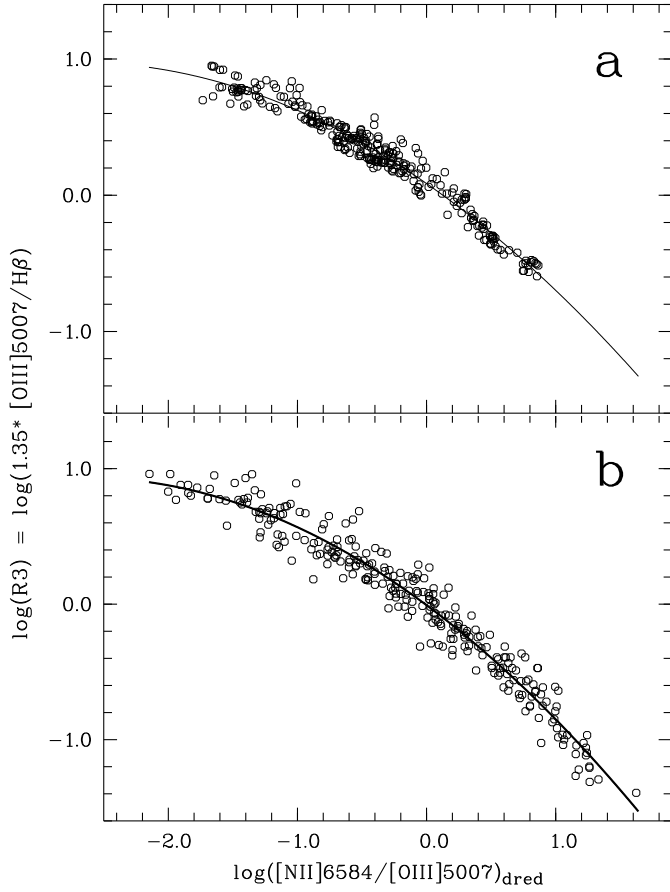


**Fig. 3.** Relations between  $\log(R_3)$  and dereddened  $\log([N II]\lambda 6584/[O III]\lambda 5007)$ . **a** for the HII regions in our sample of starburst galaxies that are not affected by Balmer absorption. **b** for 278 HII regions in normal galaxies, from the samples of McCall et al. (1985) and Vila-Costas et al. (1993). The two continuous lines in **a** and **b** are adjusted polynomials

(1985) and of Vila-Costas & Edmunds (1993). As shown in Fig. 3b, the behavior is the same. Fitting a two-degree polynomial we obtain:

$$\log(R_3) = -0.133 (\log([N II]/[O III]))^2 - 0.709 \log([N II]/[O III]) - 0.008 \quad (7)$$

The dispersion in  $\log(R_3)$  is 0.12 dex, that is slightly higher than for our sample.

It is important to note that the two fitted curves in Fig. 3 differ by a horizontal shift of 0.14 dex. This shift is consistent with the overabundance of nitrogen in SBNGs with respect to normal HII regions (Coziol et al., 1999a). Consequently, there is no unique relation between  $\log(R_3)$  and  $\log([N II]/[O III])$ , but specific relations for homogeneous samples of galaxies, such as normal ones or SBNGs. For a given value of the ratio  $[N II]/[O III]$ , a starburst galaxy will have a lower oxygen abundance than a normal galaxy, or, for a given abundance, a starburst galaxy will have a higher  $[N II]/[O III]$  ratio than a normal galaxy.

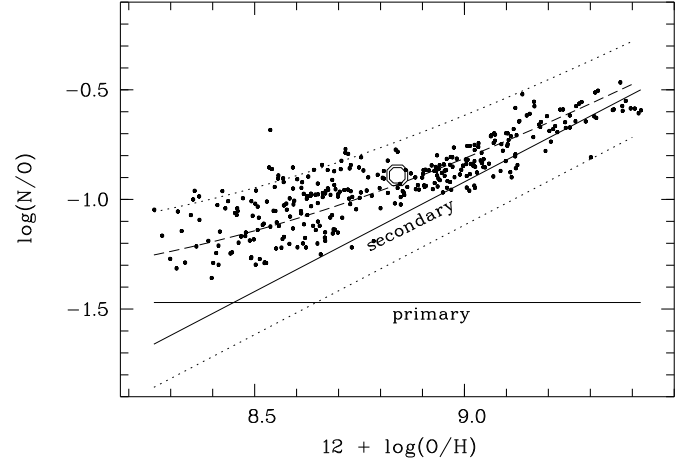


**Fig. 4.** N/O abundance ratio as a function of oxygen abundance for the HII regions in the sample galaxies. The different lines indicate the relation for *primary*, *secondary* and *primary + secondary* (dashed curve) origin of nitrogen (Vila-Costas & Edmunds 1993). The solar value is indicated by a large double circle. The two dotted curves are envelopes corresponding to the observational errors.

Figure 3a shows that our data do not reach oxygen abundances as high as in normal galaxies. This is precisely the domain where we cannot determine  $R_3$  in the standard way, because, in starburst galaxies, such high values for oxygen abundance are observed only in the nuclear regions, which are affected by Balmer absorption features. Fortunately, the parallel empirical relation for normal HII regions (Fig. 3b) continues smoothly into the high oxygen-abundance regime. We therefore consider it legitimate to use Eq.6 to calculate  $R_3$  in this range of oxygen abundances.

#### 5.4. Calculating $R_{23}$ and O/H in the center of galaxies

Once we know  $c_{H\beta}$  in the center of the sample galaxies (using Eq. 5), it is relatively easy to estimate  $R_{23}$ . First, we correct  $[O III]\lambda 5007$ ,  $[O II]\lambda 3727$  and  $H\alpha$  for reddening using  $c_{H\beta}$  and estimate the dereddened  $H\beta$  flux using the theoretical Balmer decrement:  $H\beta_{dred} = H\alpha_{dred}/2.85$ . Then, the dereddened ratio  $R_{23}$  is computed assuming  $[O III] = 1.35 \times [O III]\lambda 5007$ , and the oxygen abundance O/H is deduced using the relation of Vacca & Conti (1992).

Comparing the abundances obtained using  $R_3$  and  $R_{23}$  in the center of galaxies, we find the same kind of sensitivity to dust extinction as that observed in the outer parts of galaxies. Consequently, we also adopt the average value of the oxygen abundances estimated by  $R_3$  and  $R_{23}$  in the center of our sample galaxies.

#### 5.5. N/O abundance ratios

With the data at hand, it is possible to derive the nitrogen-to-oxygen abundance ratio (N/O). For HII regions in our sample,

**Table 2.** Observed gradients and intersects in O/H and N/O

Galaxy Mrk #	O/H				N/O			
	Global (dex/kpc)	Intersect [O/H]	Bar (dex/kpc)	Disk (dex/kpc)	Global (dex/kpc)	Intersect N/O	Bar (dex/kpc)	Disk (dex/kpc)
2	$-0.034 \pm 0.022$	$+0.31 \pm 0.03$	$-0.034 \pm 0.022$		0.000	$-0.63 \pm 0.07$	0.000	
12	$-0.093 \pm 0.007$	$+0.16 \pm 0.08$	$-0.071 \pm 0.008$	$-0.081 \pm 0.010$	$-0.037 \pm 0.008$	$-0.91 \pm 0.10$	0.000	$-0.041 \pm 0.012$
13	$-0.438 \pm 0.047$	$-0.09 \pm 0.04$	0.000	$-0.510 \pm 0.082$	0.000	$-1.14 \pm 0.04$	0.000	0.000
306	$-0.041 \pm 0.007$	$-0.18 \pm 0.07$	$-0.078 \pm 0.004$	0.000	$-0.037 \pm 0.009$	$-1.08 \pm 0.09$	0.000	0.000
307	$-0.114 \pm 0.011$	$+0.21 \pm 0.11$	$-0.098 \pm 0.025$	$-0.059 \pm 0.021$	$-0.040 \pm 0.008$	$-0.76 \pm 0.09$	0.000	$-0.037 \pm 0.019$
326	$-0.269 \pm 0.027$	$+0.49 \pm 0.10$	$-0.305 \pm 0.047$	0.000	$-0.154 \pm 0.023$	$-0.56 \pm 0.11$	$-0.124 \pm 0.048$	0.000
332	$-0.169 \pm 0.017$	$+0.39 \pm 0.12$	$-0.175 \pm 0.056$	$-0.242 \pm 0.028$	$-0.057 \pm 0.007$	$-0.76 \pm 0.04$	$-0.072 \pm 0.023$	$-0.050 \pm 0.012$
373	$-0.030 \pm 0.012$	$-0.12 \pm 0.05$	$-0.045 \pm 0.018$		$-0.071 \pm 0.021$	$-0.80 \pm 0.09$	$-0.097 \pm 0.025$	
545	$-0.014 \pm 0.008$	$+0.04 \pm 0.12$	$-0.248 \pm 0.045$	0.000	0.000	$-0.91 \pm 0.08$	$-0.035 \pm 0.015$	0.000
602	$-0.113 \pm 0.015$	$+0.21 \pm 0.14$	$-0.114 \pm 0.052$	0.000	$-0.095 \pm 0.016$	$-0.68 \pm 0.16$	$-0.147 \pm 0.033$	$-0.129 \pm 0.048$
710	$-0.119 \pm 0.049$	$+0.23 \pm 0.08$	$-0.119 \pm 0.049$					
712	0.000	$-0.40 \pm 0.06$	0.000					
799	$-0.086 \pm 0.010$	$+0.54 \pm 0.12$	$-0.116 \pm 0.021$	$-0.062 \pm 0.035$	$-0.039 \pm 0.008$	$-0.64 \pm 0.09$	$-0.036 \pm 0.019$	$-0.098 \pm 0.031$
898	$-0.184 \pm 0.010$	$+0.55 \pm 0.02$	$-0.184 \pm 0.010$		0.000	$-0.58 \pm 0.14$	0.000	
1076	$-0.131 \pm 0.010$	$+0.19 \pm 0.02$	$-0.131 \pm 0.010$		$-0.038 \pm 0.020$	$-0.85 \pm 0.05$	$-0.038 \pm 0.020$	
1088	$-0.061 \pm 0.009$	$+0.47 \pm 0.09$	0.000		$-0.027 \pm 0.006$	$-0.65 \pm 0.06$	0.000	

the N/O abundance ratio has been derived from the dereddened emission lines [O II] $\lambda$ 3727, [O III] $\lambda$ 5007 and [N II] $\lambda$ 6584 following the method of Thurston et al.(1996), as described in Coziol et al. (1999a).

The N/O abundance ratio as a function of oxygen abundance is shown in Fig. 4. Also shown in this figure are the expected relations for a *primary*, a *secondary* and a *primary + secondary* origin for the production of nitrogen (Vila-Costas & Edmunds, 1993). The HII regions in our sample seem to follow the *primary + secondary* relation. But the evolution of N/O with oxygen abundance does not trace a continuous behavior: it suddenly rises and forms a sort of plateau between  $8.7 < 12 + \log(\text{O/H}) < 9.1$ . This behavior has been interpreted as evidence for chemical evolution by a sequence of bursts of star formation (Coziol et al. 1999a).

## 6. Results

### 6.1. Spatial distribution of oxygen abundances and of H $\alpha$

The oxygen abundance and H $\alpha$  emission as a function of position along the slit are presented in Fig. 5. The emission peak is usually centered on the nucleus of galaxies. Exceptions are Mrk 12, 13, 712 and 799. In the case of Mrk 712 and 799, the maximum intensities correspond to very young star-forming regions containing numerous Wolf-Rayet stars. When studying the gas distribution inside the bar, we find two possible situations: more than half of galaxies have ionized gas covering the whole bar, while in the rest of galaxies the ionized gas is mostly confined to the center. A large number of galaxies (62%) also show ionized gas either at the two ends of the bar (25%), or, more frequently, only at one end (37%).

Examining the spatial distribution of the oxygen abundance, we find that it usually reaches a maximum in the center of galaxies. In general, this maximum corresponds to that of the H $\alpha$  emission. In some galaxies, there is also strong nebular emission outside the nucleus, accompanied by a local rise in

oxygen abundance (e.g. Mrk 306, 332 and 545). In other galaxies this secondary peak of emission is not accompanied by an increase in oxygen abundance (e.g. Mrk 12, 13 and 799), and in some galaxies the oxygen abundance stays high even without any secondary peak of H $\alpha$  emission (e.g. Mrk 307, 373 and 712).

### 6.2. O/H and N/O abundance gradients

To study the abundance gradients, we have folded the profiles of O/H and N/O abundance ratios about a center of symmetry. This center is the locus of the principal peak of H $\alpha$  emission (see Fig. 5).

To make the analysis easier, we adjusted lines by least-square fits to the data in two different regions of each profile: one includes the bar and the nucleus and another the region outside the bar. The latter region corresponds to the disk. Note, however, that the profiles never cover the entire length of the disk (that is out to a surface brightness of 25 mag arcsec $^{-2}$ ), simply because we did not detect ionized gas that far. A global gradient is also estimated by fitting a line to the data over the full extent of the ionized gas distribution. The intersect (central) abundance is determined by extrapolating this global gradient up to the center. The two regressions are plotted as continuous lines and the global gradient as a dotted line in Figs. 6 and 7. The profiles on the two sides of the center are distinguished by different symbols. The numerical values of different gradients and the intersects are given in Table 2. The uncertainties reported in that Table are those obtained from the regression calculations.

The oxygen abundance profiles as a function of radius (in arcsec) are shown in Fig. 6. They show complicated patterns. Although the uncertainties on the oxygen abundance ( $\sim 0.2$  dex) prevent us from interpreting the multiple inflections of these profiles, we believe that part of these features must be real, reflecting variations in oxygen abundance produced by

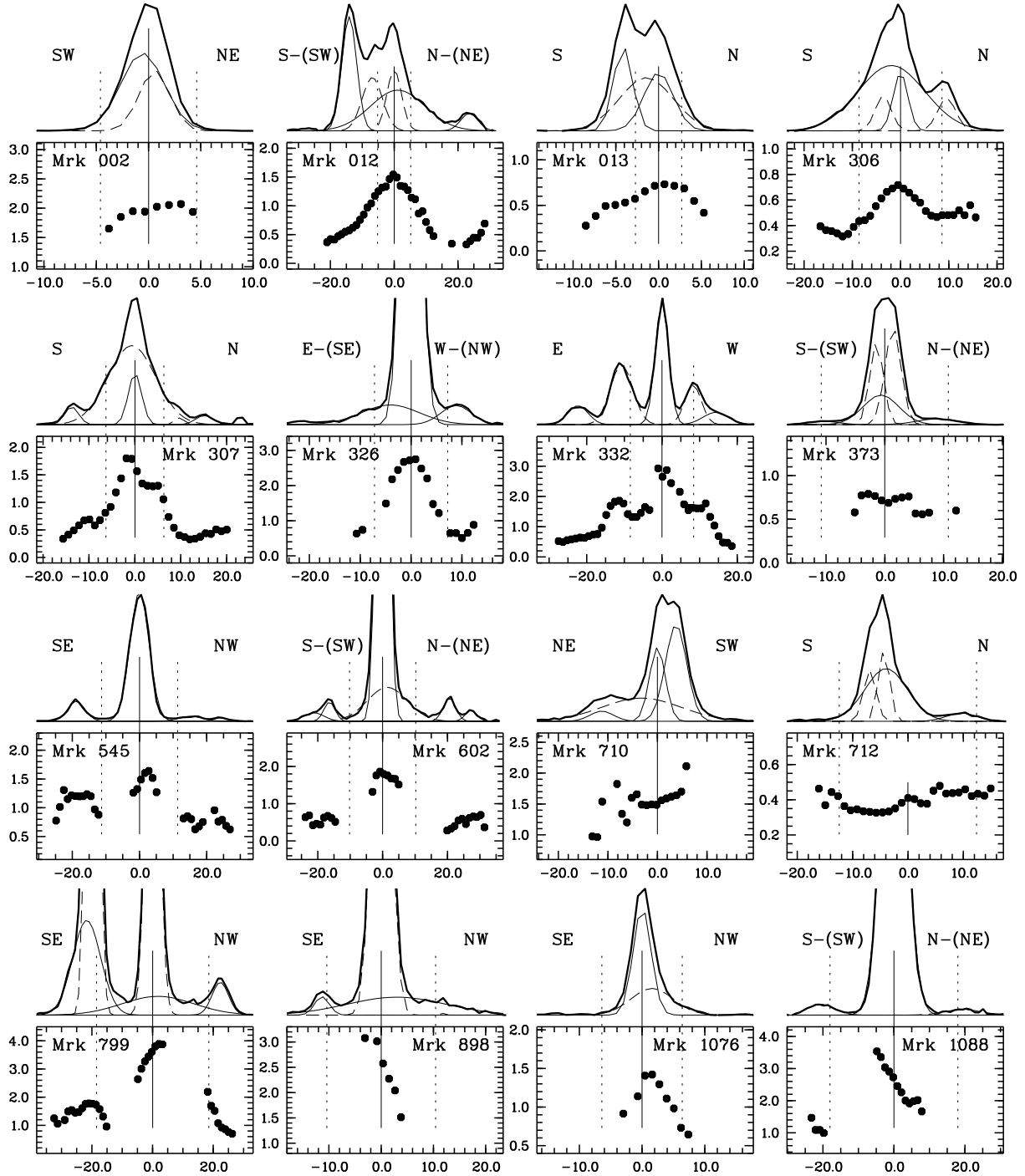


**Fig. 5.** The oxygen abundance and  $H\alpha$  emission of the galaxies versus position along the slit in arcsec. The oxygen abundance is given in solar units, adopting  $\log(O/H) = -3.16$  for the solar value (Grevesse & Noels 1993). For each galaxy, a vertical continuous line marks its geometrical center and two vertical dotted lines indicate the two ends of the bar. In Mrk 710 the ends of the bar fall outside the figure (at 33.7 arcsec). When the spatial  $H\alpha$  profile is not a pure gaussian, we also draw its decomposition into multi-gaussian components

different intensities of star formation along the bar. One good example is Mrk 332, where there is an increase of oxygen abundance linked to star formation at the two ends of the bar.

The abundance gradients (continuous and dotted lines in Fig. 6) also show various patterns. In Mrk 2, 373, 710, 712, 898 and 1076, the gradient can be estimated in the bar only. In these cases, the bar gradient is considered the global gradient.

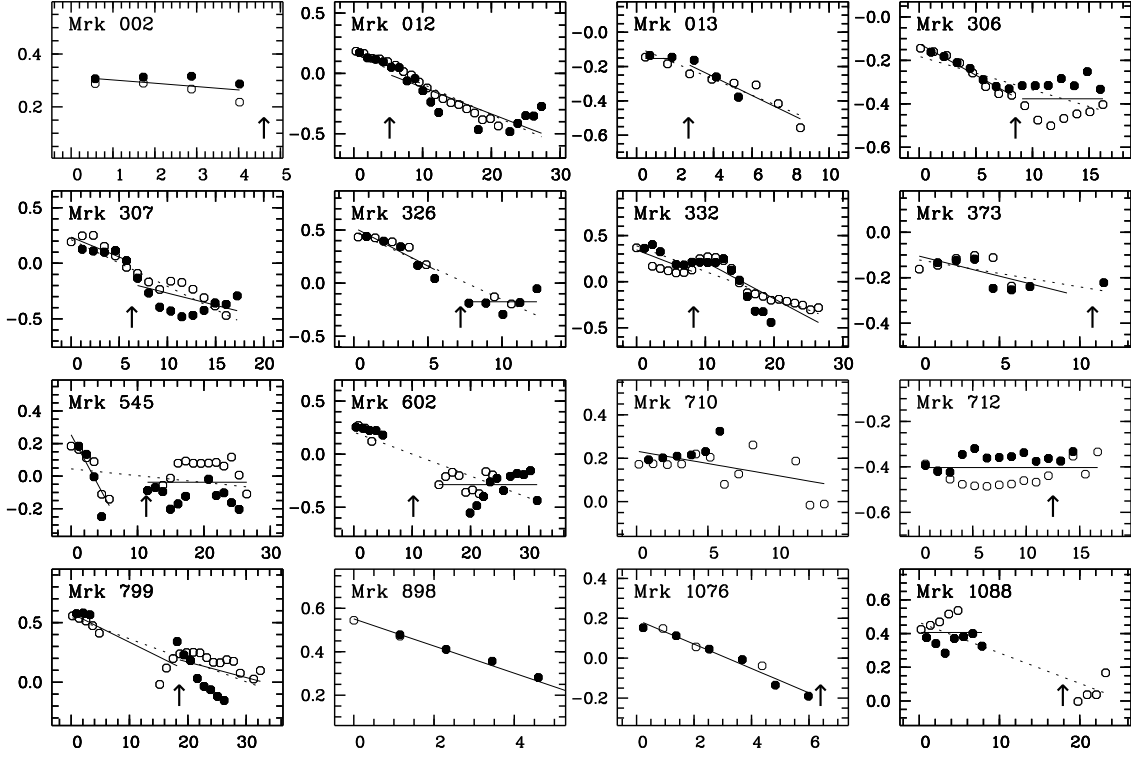


**Fig. 6.** Radial profiles of oxygen abundance  $\log(\text{O}/\text{H})$  in solar units. The radial coordinate is in arcsec, with the origin at the center of symmetry of the profile. Values on both sides of the center are distinguished by two different symbols. In each panel the vertical arrow indicates the end of the bar. The slopes of the lines adjusted by least-square fits are given in Table 2. The two continuous lines correspond to the bar and disk abundance gradients and the dotted line corresponds to the global gradient

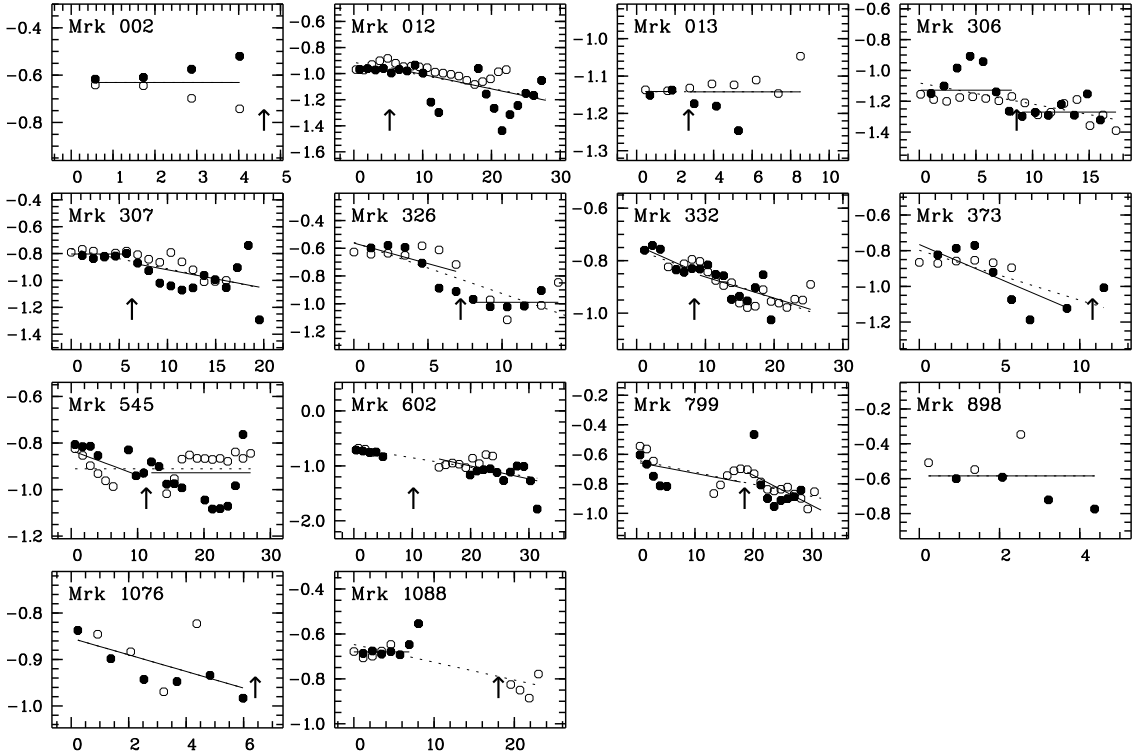


**Fig. 7.** Radial profiles of nitrogen-to-oxygen abundance ratio  $\log(\text{N}/\text{O})$ . The solar value on this scale corresponds to  $-0.9$ . The meaning of the symbols is the same as in Fig. 6. The slopes of the lines adjusted by least-square fits are given in Table 2



Half of these gradients are relatively shallow ( $\sim -0.03$ ) and half are moderately strong ( $\sim -0.15$ ).

For galaxies with ionized gas also in the disk, we distinguish two cases: the disk abundance gradient can be either flat or negative. In Mrk 306, 326, 545 and 602, it is flat. Considering that normal spiral galaxies usually have monotonous negative gradients (Zaritsky et al., 1994), this makes these galaxies with flat disk gradient somewhat peculiar, although shallower outer profiles have been observed before, for instances in NGC 1365 (Roy & Walsh, 1998), NGC 3319 (Zaritsky et al., 1994) and NGC 3359 (Martin & Roy, 1995). Other galaxies with ionized gas in the disk look more “normal”, with negative disk gradients. In general, the gradients are shallower in the disk than in the bar. There are two exceptions, Mrk 13 and Mrk 332. In the case of Mrk 332, the intense star formation located at the ends of the bar is obviously responsible for the steeper gradient in the disk (see Fig. 6). For Mrk 13, there is no gradient in the bar simply because this bar is very short, it is the shortest bar among the 125 ones measured by Chapelon et al. (1999) (paper V). The bar of Mrk 1088 also seems to have a flat gradient (Fig. 6), but the unfolded oxygen abundance profile (Fig. 5) shows that there is in fact a steep gradient *across* the center.

In general, our global abundance gradients are negative. This reflects the fact that the oxygen abundance is almost always highest in the center of the galaxy. One exception is Mrk 712, which does not have any gradient at all.

We determined the N/O abundance ratios of all galaxies except Mrk 710 and 712 (see Sect. 5.5). The N/O profiles are shown in Fig. 7. In general, they look similar to those of oxygen. The N/O abundance ratio also increases toward the nucleus of the starburst galaxies, but the gradients are significantly shallower and many more galaxies have zero gradient. Further comparisons of the two abundance gradients are postponed to Sect. 7. Values for the different gradients and the intersects are given in Table 2.

## 7. Analysis of the abundance gradients

### 7.1. Oxygen abundance gradients

The presence of a bar could affect the abundance gradients in our sample of galaxies in two ways. By funneling metal-poor gas from the outer regions toward the center, the bar is expected to dilute the chemical elements, and thus reduce any initially present radial abundance gradient. But a bar could also stimulate star formation at the centre, which, if strong enough, could establish or maintain a steep abundance gradient. In the following analysis, we look for such possible effects of the bar in our sample of starburst galaxies.

Of the three categories of oxygen abundance gradients estimated here, the global gradient is the one which is most comparable to those from other studies. We show in Fig. 8 the relation of global gradients and intersects with absolute magnitudes. This Figure should be compared with Fig. 1 of Edmunds & Roy (1993) for a sample of normal galaxies. The barred starburst galaxies generally have steeper gradients than normal barred

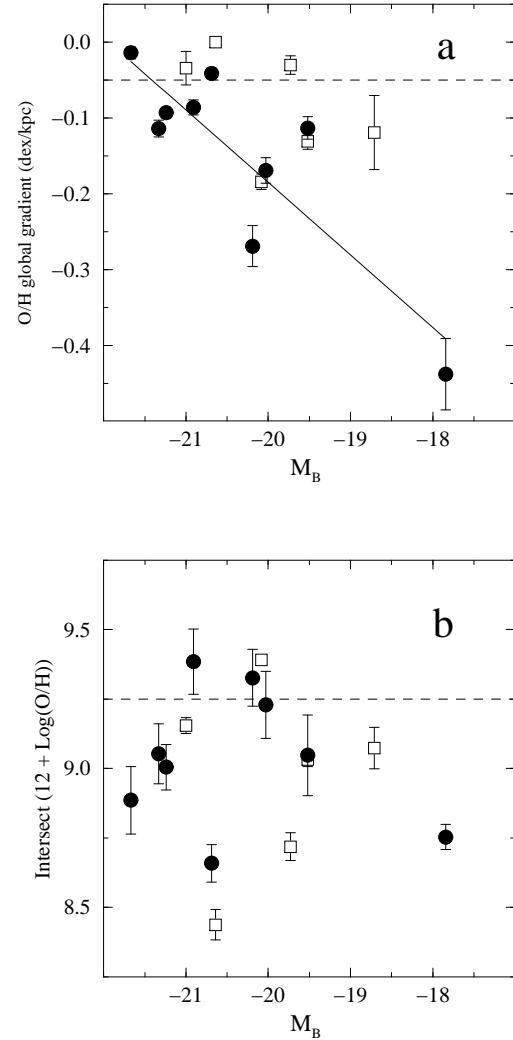


**Fig. 8.** **a** Global oxygen abundance gradient as a function of absolute magnitude. Galaxies where the global gradient is also the bar gradient are indicated by open squares; filled circles represent the other cases. The dashed line marks the mean gradient of normal unbarred galaxies with absolute B magnitude between  $-19$  and  $-22$  in the sample of Edmunds & Roy (1993). The continuous curve is a linear regression on the filled circles (correlation coefficient = 86%). **b** Intersect as a function of the absolute magnitude. The meaning of the symbols is the same as in **a**. The dashed line indicates a mean value of the central oxygen abundance in normal unbarred galaxies with absolute B magnitude between  $-19$  and  $-22$  (from Edmunds & Roy 1993)

galaxies (Edmunds & Roy, 1993; Zaritsky et al., 1994). On average, the gradients in the barred starburst galaxies are even steeper than those measured by Edmunds & Roy (1993) in normal unbarred galaxies of comparable luminosity. This shows that the oxygen abundance in the sample of barred starburst galaxies is not diluted by the mixing effect of the bar.

In the above analysis, six of the global abundance gradients are in fact bar gradients, because no ionized gas was ob-

served in the disks of these galaxies. We should therefore re-examine Fig. 8 and distinguish these cases from those where the global gradient includes the disk gradient. With this distinction, we find that the global gradient in Fig. 8a tends to steepen as the absolute magnitude increases. A linear fit performed on the data yields a correlation coefficient of 86%. But if we exclude the extreme point (Mrk 13) at  $M_B \sim -18$ , this coefficient drops to 56%. This is more a trend than a true correlation. Galaxies for which the global gradient is the bar gradient also show a similar trend, but slightly displaced towards lower values. An explanation for this trend is proposed in Sect. 8.2.

Examining now the central oxygen abundances (Fig. 8b), we find that they are on average lower in barred starburst galaxies than in normal unbarred galaxies. Because the global abundance gradients in barred starburst galaxies are strong, these low central abundances cannot be attributed to an artifact of the bar, that would have lowered the central abundance of chemically evolved galaxies by dilution. This means that the starburst galaxies in this sample have lower oxygen abundances than normal ones. This is in agreement with our previous finding (Coziol et al., 1997a; Coziol et al., 1998): SBNGs are chemically less evolved than normal galaxies with comparable luminosity and morphology. We have shown elsewhere (Coziol et al., 1997a; Coziol et al., 1998), that the only way to explain this phenomenon is by assuming that SBNGs are “young” galaxies.

### 7.2. N/O abundance gradients

We have shown that trends in the oxygen abundance gradients are inconsistent with the mixing effect of a bar, unless the bar also triggers a central starburst which more than compensates for the dilution. However, the fact that we find both strong oxygen abundance gradients and lower intersects than in normal galaxies rules out a bar-triggered burst in the center of an “old” galaxy.

But the bar could be responsible for starbursts in the center of a relatively “young” galaxy. In this case, there are two alternatives. The gas funneled by the bar could have been fed directly into the central region in a short time (a few Myrs), prompting a new burst of star formation that is sufficiently strong to produce steep abundance gradients. The other alternative is that the bar acts over a much longer time scale (a few Gyrs), progressively feeding the inner regions with gas that is immediately recycled (since no mixing effects are seen).

We can test the above two alternatives by studying the N/O abundance gradients and comparing them with the oxygen ones. In Coziol et al. (1999a), we have shown that the bulk of nitrogen in SBNGs is probably produced by intermediate-mass stars, whereas oxygen is mainly released by massive stars. In this scenario, the time scale for enrichment in nitrogen ( $400 \text{ Myr} < \tau < 2 \text{ Gyr}$ ) is much longer than the one for oxygen ( $\tau < 20 \text{ Myr}$ ). This allows us to look for effects of the bar on a time scale covering a few Gyrs.

In Fig 9a, we show the relation between the global N/O abundance gradient and absolute magnitude. In this Figure, we distinguish galaxies with a gradient measured only along the

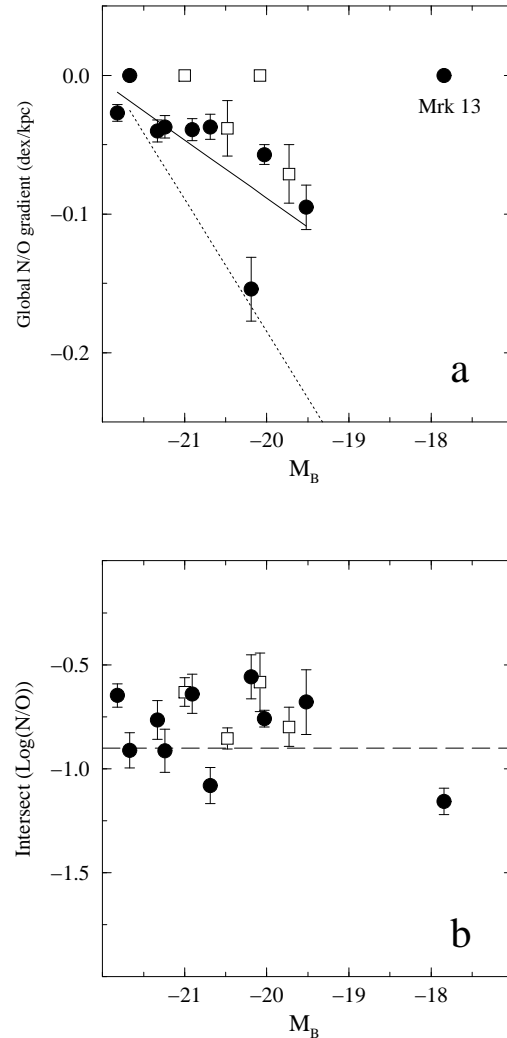


**Fig. 9.** **a** Global N/O gradient as a function of absolute magnitude. The symbols have the same meaning as in Fig. 8. The continuous line is a regression on the N/O values, with a correlation coefficient of 75%. For the sake of comparison, we also give the linear regression (dotted line) obtained for the gradient in O/H (see Fig. 8). **b** Intersect as a function of absolute magnitude. The horizontal dashed line corresponds to the solar value of N/O

bar from those where the gradient also includes the disk. We observe the same trend for N/O as for oxygen: galaxies with a lower luminosity seem to have a stronger negative gradient. The relation implied by this tendency has a weak correlation coefficient (60% with Mrk 13 excluded) and a shallower slope than that found for oxygen. Again, galaxies with only a bar gradient seem to have shallower gradients than the other ones.

Despite the small gradients, the central N/O values, shown in Fig. 9b, are rather high compared to the solar abundance. This implies that many generations of intermediate-mass stars have already contributed to enrich these galaxies in nitrogen, or, equivalently, that enough time has passed in the chemical evolution of these galaxies.

Why is the gradient systematically weaker for N/O than for oxygen? If this is due to the bar, it means that the effect of the bar appears on a time scale comparable to the nitrogen enrichment phase. This is unlikely as it implies that the oxygen enrichment phase, and the ensuing strong oxygen abundance gradient, happened after the nitrogen one. Therefore, as a mixing mechanism, the bar should have affected both elements in the same way, which is not observed. Our explanation for the observed difference is given in Sect 7.3.

The fact that the N/O intersects are high rules out the possibility that the bars recently triggered central starbursts in these galaxies. A recent burst would have increased the oxygen abundance and decreased the N/O abundance ratio. The stronger the burst, the stronger the decrease in N/O. We would thus expect galaxies with the steepest oxygen abundance gradients to have the flattest N/O ones. In Fig. 10a, we show the relation between the oxygen and N/O abundance gradients. The behavior is contrary to what is expected. The bars consequently did not recently trigger bursts in these galaxies.

### 7.3. The progressive build up of abundance gradients

What is then the reason for the difference between the two gradients? In fact, the N/O abundance gradient is not independent of the oxygen one. This is shown in Fig. 10a. A linear regression on the data yields the relation:  $\Delta(\text{N/O})/\Delta r = 0.53 (\pm 0.10) \Delta(\text{O/H})/\Delta r + 0.00 (\pm 0.01)$  with a correlation coefficient of 89%. Surprisingly, the slope of this relation is almost the same as the one found between the N/O and oxygen abundances: a linear fit performed on the data in Fig. 4 yields  $\log(\text{N/O}) = 0.55 \log(\text{O/H}) + 0.8$  (Coziol et al., 1999a), which is consistent with a mixture of *primary* + *secondary* origin for nitrogen (McGaugh, 1991).

The relation between the two gradients is thus explained by the behavior of the oxygen abundance in the nuclei of the galaxies. This is shown in Fig. 10b, where the oxygen abundance gradient steepens when its intersect increases. This relation is trivial if we assume that all disks initially have about the same low oxygen abundance (see Fig. 6). Since the nitrogen enrichment is related to the increase in oxygen (See Sect. 5.5 and Fig. 4), the N/O abundance gradient grows with that of oxygen. The origin of both gradients in starburst galaxies can thus be explained solely by their star formation histories.

## 8. The role of bars in starburst galaxies

The only way to reconcile the above observations of abundance gradients with the possible effect of a bar is by assuming that the latter is a slow process; over a few Gyr period, the bar progressively feeds the nucleus with gas which is immediately recycled into stars. This scenario requires a very fine tuning between the feeding of the gas in the center of galaxies and star formation. It also requires that bars are relatively stable over a long period of time (a few Gyrs). We can test if these conditions apply to galaxies in our sample by looking for relations between the bar properties and star formation.

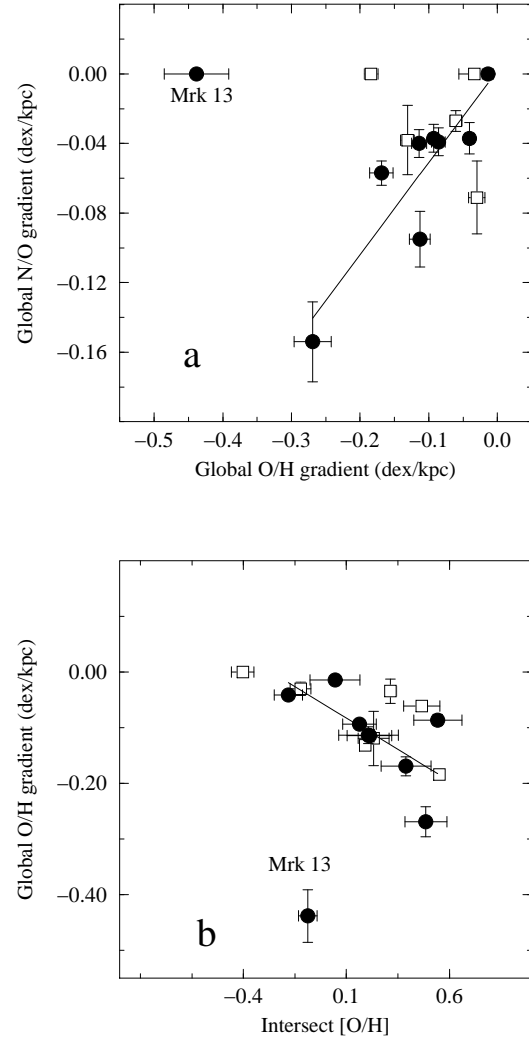


**Fig. 10.** **a** Relation between global gradients in N/O and O/H. The symbols have the same meaning as in Fig. 8. The continuous curve is a linear regression with a correlation coefficient of 89%. **b** Relation between the global gradients in O/H and its intersect. The continuous curve is a linear regression with a correlation coefficient of 68%

### 8.1. Bar properties and star formation: evidence for young bars

Numerical simulations predict that a strong bar maintains a steeper abundance gradient in the bar than in the disk for about 1 Gyr, then both become comparably low ( $\sim -0.02$ ), and that the bar and disk gradients are never very different in the presence of a weak bar (Martinet & Friedli, 1997). We show in Fig. 11 that almost all galaxies in our sample show a stronger gradient in the bar than in the disk. Only two galaxies, Mrk 13 and 332, have significantly steeper gradients in the disk than in the bar, but this peculiarity can be explained by other phenomena (see Sect. 6.2). In other words, the difference between bar and disk gradients cannot be due to an old bar. It cannot be due to the effect of a young bar either, because, as we pre-

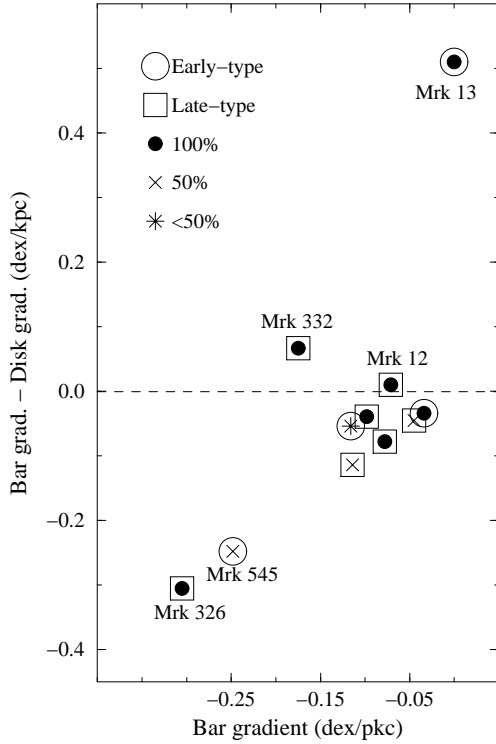


**Fig. 11.** Difference between oxygen abundance gradients in the bar and in the disk. The difference is shown as a function of the gradient in the bar, which explains why the galaxies with a bar gradient only follow a 1 to 1 relation. The galaxies with ionized gas over the whole bar (●) are distinguished from those where the gas covers 50% (×) or less (\*) of the bar. Early-type galaxies are indicated by a large open circle and late-type ones by a large open square

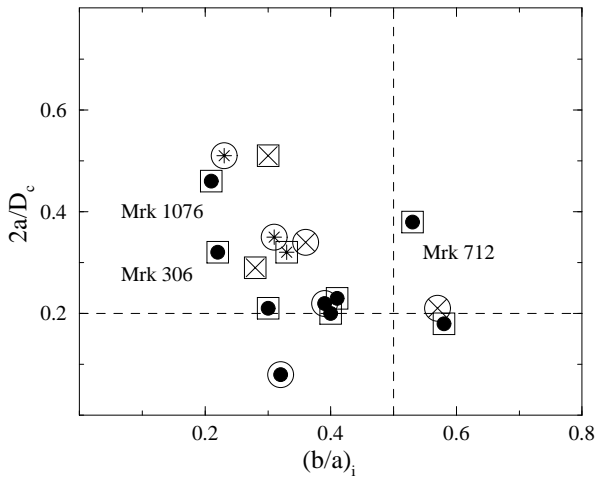


**Fig. 12.** Distribution of ionized gas along the bar as a function of bar and galaxy morphologies. The symbols have the same meaning as in Fig. 11. The horizontal and vertical dashed lines indicate the limits of short and weak bars respectively. There is a tendency for the ionized gas to be less extended in longer bars

viously noted, the N/O abundance ratios would be low and the gradients would be anti-correlated.

A simple explanation for the stronger gradients in the bar than in the disk is that the volume density of star formation is proportional to the gas volume density to some power  $n$  ( $1 \leq n \leq 2$ ), as proposed by Schmidt's law (1959, 1963). Assuming that the chemical enrichment is proportional to the star formation, a spherical density distribution yields a variation with radius in  $R^{-3/n}$ . The gradient measured from the center to the end of the bar (or to any intermediate radius) will necessarily be steeper than the one measured further out.

The presence of ionized gas is a tracer of star formation in galaxies. Half the galaxies in this sample show the presence of ionized gas over the whole bar, while in the other half, the gas is mostly concentrated in the inner parts of the bar and in the nucleus. If star formation cannot result from gas flow toward the inner regions by the dynamical action of a bar, could it be linked to any other property of the bar, such as its strength or its length? The bar strength is identified with the deprojected bar axis ratio  $(b/a)_i$ , and its length is given by the ratio of the deprojected major axis to corrected blue isophotal diameter  $2a/D_c$  (Chapelon et al., 1999) (Paper V). A bar with a ratio  $b/a < 0.5$  is considered “strong” and a bar with a ratio  $2a/D_c > 0.2$  is considered “long”. We also identify separately galaxies with various fractions of ionized gas along the bar and galaxies with early- (earlier than SBbc) or late-type (SBbc or later) morphologies.

As shown in Fig. 12, most galaxies in this sample have a strong bar, which is a general characteristic of the sample of Markarian barred starburst galaxies (Chapelon et al., 1999). There is a trend for galaxies with a longer bar to have ionized gas over a smaller extent of the bar length, regardless of their morphology. This is not an observational selection effect, because three galaxies do not follow the above trend in Fig. 12, namely Mrk 306, 712 and 1076. In the case of Mrk 306 and 1076, a long and strong bar with ionized gas over its whole length may be explained by the fact that they are both interacting with close companions (the rest of our galaxies are isolated). Mrk 712 looks like an isolated galaxy, but with a peculiar morphology. The peak of star forming activity is significantly displaced from the center of the galaxy (see Fig. 5). This active region may be associated with a second nucleus (Mazzarella & Boroson, 1993), which makes this galaxy a strong candidate for a recent merger. A simple relation with the length of the bar thus explains the radial distribution of ionized gas; star formation does not cover the whole bar just because it is too long.

We have shown so far that bars, despite the fact that they are strong, cannot account for the observed abundance gradients. This may be surprising in view of the convincing evidence for dynamical effects of strong bars on star formation and abundance gradients in galaxies provided by numerical simulations. The only explanation for such a situation is that bars in the current sample of galaxies are too young (a few  $10^7$  years) to have had any effect.

We verified that there are no relations between the abundance gradients and the bar properties. The oxygen and N/O abundance gradients in the bar and in the disk show the same behavior. No relation is found between the abundance gradients and the bar strength or length. Nor is any relation found between the abundance gradients and the different concentrations of gas along the bar. In general, therefore, the bars have not influenced the two gradients. This supports our assumption that the bars are young.

### 8.2. Bar-induced star formation at the bar ends

If we compare the distribution of ionized gas (i.e. star formation) with the oxygen abundance, we find that the behaviors of these two parameters along the bars are frequently uncorrelated (see Fig. 5 and Sect. 6.1). Intense star formation does not necessarily enhance the oxygen abundance, as we can see, for example, in the extranuclear star forming regions of Mrk 12 and 799. These regions must be too young (a few Myrs) and their massive stars did not have enough time to change the chemical abundance of their environment. When we find, on the other hand, a region filled with ionized gas, but where the abundance is significantly higher, we conclude that this must be a region where star formation was “stable” over a longer period of time. The galaxy nuclei in our sample are obvious locations for such stable star-forming regions. The relatively high N/O abundance ratios and the high proportion of intermediate-mass stars mixed with ionized gas indicate that star formation persisted in these regions for quite a long time (a few Gyrs).

We found no evidence that bars triggered the starbursts observed at the center of the sample galaxies. On the other hand, they may have induced star formation at the ends of the bar (e.g. Mrk 307, 332), and more frequently at only one end (e.g. Mrk 12, 13, 306, 545 and 799). This phenomenon may be due to gas compression in these regions (Roberts et al., 1979). Star formation induced by the bar at its ends has increased the oxygen abundance there. The result is a shallower abundance gradient in the bar and a stronger one in the disk. This may explain why the global oxygen and N/O abundance gradients are weaker when they are measured only in the bar. Chemical enrichment produced by star formation at these points being lower than what is observed in the nucleus, this suggests that fewer star formation episodes occurred there, or that they happened relatively recently.

Among all the possible effects of the bar on the evolution of starburst galaxies, therefore, the only plausible one seems to be star formation induced at one or both ends of the bars. The distribution of star formation in this sample of starburst galaxies is consistent with the assumption that bars are too young (a few  $10^7$  years old) to be at the origin of the bursts in the galaxy nuclei.

## 9. Summary and conclusion

One important result of our analysis is that bars have not had a great impact on the star formation history and chemical evolu-

tion of starburst galaxies. The most straightforward explanation is that bars are too young. Our observations also clearly show that these young bars cannot be at the origin of the nuclear starbursts. The high N/O abundance ratios together with the high level of star formation in the nuclear region of galaxies suggest that star formation proceeds almost steadily (or as a sequence of bursts) over a few Gyr period.

The fact that we find strong O/H gradients while the oxygen abundance is low in the galactic nuclei supports our interpretation that SBNGs are young galaxies still in their process of formation (Coziol et al. 1997a; 1997b). It seems that these starburst galaxies are still building their abundance gradients. This process can be fully explained in terms of their star formation history. The gradients build up from the inside out, becoming stronger as the oxygen and N/O abundances increase in the bulge while staying low in the disk. This behavior is consistent with a simple Schmidt law relating the density of star formation to that of gas.

According to these results, starburst galaxies seem to form their bulge first, and then their disk. If the disk is younger than the bulge and the bar forms in the disk, it is not surprising that we find mostly young bars in starburst galaxies. The above scenario may also explain why our results are not consistent with predictions made by different models of bar formation. The initial conditions assumed in these models are far from those observed in young starburst galaxies. A bar forms in a galaxy which already has a large bulge but a disk which is probably still in formation.

When star formation stops in the bulge and increases in the disk, as in normal spiral galaxies, the metallicity of the disk grows, decreasing the gradient. If the end product of a starburst galaxy is a normal spiral galaxy, the latter, therefore, should have lower metallicity gradients than the former. If they are stable, bars may also play a more important role as galaxies get older.

But how general is our conclusion? Is what we observe a trait of SBNGs? What is the relation between the bulge and disk formation in starburst galaxies and in normal spiral galaxies? These are the questions we address in our companion paper (Coziol et al. 2000).

*Acknowledgements.* We thank the staff of Observatoire de Haute-Provence for assistance at the telescope. R. C. would also like to thank Observatoire de Besançon for funding his visit, during which this paper was completed. He would also like to thank the direction and staff of Observatoire de Besançon for their hospitality. We acknowledge with thanks from the referee, Danielle Alloin, positive comments and constructive suggestions which have helped to improve the quality of this paper. For this research, we have made use of the Lyon-Meudon Extragalactic Database (LEDa), operated by the Lyon and Paris-Meudon Observatories (France). We also used the NASA/IPAC Extragalactic Database (NED) which is operated by the Jet Propulsion Laboratory, California Institute of Technology, under contract with the National Aeronautics and Space Administration.

## References

- Alloin D., Collin-Souffrin S., Joly M., Vigroux L., 1979, *A&A* 78, 5
- Baldwin J.A., Phillips M.M., Terlevich R., 1981, *PASP* 93, 5
- Chapelon S., Contini T., Davoust E., 1999, *A&A* 345, 81 (Paper V)
- Contini T., 1996, Ph. D. thesis, Université Paul Sabatier, Toulouse, France
- Contini T., Davoust E., Considère S., 1995, *A&A* 303, 440 (Paper I)
- Contini T., Wozniak H., Considère S., Davoust E., 1996, in Proceedings of the workshop “The physics of LINERs in view of recent observations”, *ASP Conference series*, 103, 175
- Contini T., Wozniak H., Considère S., Davoust E., 1997, *A&A* 324, 41 (Paper II)
- Contini T., Considère S., Davoust E., 1998, *A&AS* 130, 285 (Paper III)
- Coziol R., 1996, *A&A* 309, 345
- Coziol R., Contini T., Davoust E., Considère S., 1997a, *ApJ* 481, L67
- Coziol R., Demers S., Barnéoud R., Pena M., 1997b, *AJ* 113, 1548
- Coziol R., Contini T., Davoust E., Considère S., 1998, in *Abundance Profiles: Diagnostic Tools for Galaxy History*, Eds.: D. Friedli, M. Edmunds, C. Robert, L. Drissen, *ASP Conf. Ser. Vol. 147*, (San Francisco) p. 219.
- Coziol R., Carlos-Reyes R.E., Considère S., Davoust E., Contini T., 1999a, *A&A* 345, 733
- Coziol R., Considère S., Davoust E., Contini T., 2000, submitted
- Edmunds M.G., 1990, *MNRAS* 246, 678
- Edmunds M.G., Pagel B.E.P., 1984, *MNRAS* 211, 507
- Edmunds M.G., Roy J.-R., 1993, *MNRAS* 261, L17
- Friedli D., Benz W., Kennicutt R., 1994, *ApJ* 430, L105
- Grevesse N., Noels A., 1993, in “Origin and Evolution of the Elements”, Prantzos N., Vangioni-Flam E., Cassé M. eds., Cambridge University Press, p. 15
- Götz M., Köppen J., 1992, *A&A* 262, 455
- Heckman T.M., Robert R., Leitherer C., Garnett D.R., van der Rydt F., 1998, *ApJ* 503, 646
- Lemaître G., Kohler D., Lacroix D., Meunier J.-P., Vin A., 1990, *A&A* 228, 540
- Martin P., Roy J.-R., 1994, *ApJ* 424, 599
- Martin P., Roy J.-R., 1995, *ApJ* 445, 161
- Martinet L., Friedli D., 1997, *A&A* 323, 363
- Massey P., Strobel K., Barnes J.V., Anderson E., 1988, *ApJ* 328, 315
- Mazzarella J.M., Boroson T.A., 1993, *ApJS* 85, 27
- McCall M.L., Rybski P., Shields G.A., 1985, *ApJS* 57, 1
- McGaugh S., 1991, *ApJ* 380, 140
- Mollá M., Ferrini F., Díaz A.I., 1996, *ApJ* 466, 668
- Noguchi M., 1988, *A&A* 203, 259
- Oye M.S., Kennicutt R.C.Jr., 1993, *ApJ* 411, 137
- Pagel B., 1989, *Rev. Mex. Astron. Astrof.* 18, 161
- Roberts W.W., Huntley J.M., van Albada G.D., 1979, *ApJ* 233, 67
- Roy J.-R., Walsh J.R., 1998, *MNRAS* 288, 715
- Schmidt M., 1959, *ApJ* 129, 243
- Schmidt M., 1963, *ApJ* 137, 758
- Thurston T.R., Edmunds M.G., Henry R.B.C., 1996, *MNRAS* 283, 990
- Vacca W.D., Conti P.S., 1992, *ApJ* 401, 543
- Veilleux S., Osterbrock D.E., 1987, *ApJS* 63, 295
- Vila-Costas M.B., Edmunds M.G., 1992, *MNRAS* 259, 121
- Vila-Costas M.B., Edmunds M.G., 1993, *MNRAS* 265, 199
- Wise R.F.G., Silk J., 1989, *ApJ* 339, 700
- Zaritsky D., Kennicutt R.C.Jr., Huchra J.P., 1994, *ApJ* 420, 87